Chemical Physics Letters 567 (2013) 6–13

Contents lists available at SciVerse ScienceDirect

Chemical Physics Letters

journal homepage: www.elsevier.com/locate/cplett

Ultrafast electronic relaxation and vibrational dynamics in a polyacetylene derivative

Takayoshi Kobayashi [a,b,c,*], Tsugumasa Iiyama [a], Kotaro Okamura [a], Juan Du [a,b,d,*], Toshio Masuda [e]

[a] Advanced Ultrafast Laser Research Center, University of Electro-Communications, 1-5-1, Chofugaoka, Chofu, Tokyo 182-8585, Japan
[b] Japan Science and Technology Agency, Core Research for Evolutional Science and Technology (CREST), Japan Science and Technology Agency, K's Gobancho, 7, Gobancho, Chiyoda-ku, Tokyo 102-0076, Japan
[c] Department of Electrophysics, National Chiao Tung University, 1001 Ta Hsueh Road, Hsin-Chu 3005, Taiwan
[d] State Key Laboratory of High Field Laser Physics, Shanghai Institute of Optics and Fine Mechanics, Chinese Academy of Sciences, Shanghai, China
[e] Department of Environmental and Biological Chemistry, Faculty of Engineering, Fukui University of Technology, 3-6-1, Gakuen, Fukui, Fukui 910-0505, Japan

ARTICLE INFO

Article history:
Available online 13 March 2013

ABSTRACT

Real-time vibrational spectra in a polyacetylene derivative, poly[*o*-TFMPA([*o*-(trifluoromethyl) phenyl]acetylene)] in a broad electronic spectral region were observed using a sub-7-fs laser. Using the frequencies and initial phases of vibrational modes obtained by the spectroscopy, the assignment of the wavepackets was made. From the first moment, Huang–Rhys parameters were determined for six most prominent modes, which characterize the potential hypersurface composed of multi-dimensional vibrational mode spaces.

1. Introduction

One-dimensional conjugated polymers have been of interest for the last two decades because of their characteristic properties including the tailorability by chemical synthetic processes to change the side groups and physical or physico-chemical modification processes of morphological, mechanical, electrical, and optical properties. The capability is useful for the preparation of materials with various electrooptical, optoelectrical, and photonic properties, which are of vital importance for varieties of applications, such as electroluminescent devices, nonlinear optical devices, and field-effect transistors [1–5]. Among them large ultrafast optical nonlinear property is based on the dimensionality and conjugation of the polymer [1,6]. Conjugation of π-electrons along the main chain of the polymer supports the correlated electrons to induce enhanced transition probability with a large transition dipole. This results in the large third-order nonlinearity because of the existence of the deviation from the bosonic properties of exciton due to the Pauli Exclusion Principle. Ultrafast relaxation is expected in such a one-dimensional system due to a barrierless potential between the free exciton and self-trapped exciton [7].

The combination of the large third-order nonlinearities due to the electronic correlation and the ultrafast response is quite attractive for basic techniques such as the optoelectro-switching and optical information processing. Many experimental and theoretical studies have been made to clarify the mechanism which is responsible for the macroscopic nonlinear properties characteristic of this class of materials [8]. The optical nonlinearities of the one-dimensional conjugated polymers are closely related to geometrically relaxed excitations such as a pair of solitons, and polarons, and a self-trapped exciton (STE). STE is equivalent to an exciton polaron and a neutral bipolaron, and is formed via strong coupling between electronic excitations and lattice vibrations [9]. A free exciton formed in such a one-dimensional system spontaneously relaxes within ~100 fs because of the absence of barrier between free exciton minimum and STE minimum of the potential curves [10] and change optical properties of the conjugated polymers, inducing the absorption coefficients and refractive indices [10,11]. Relaxation dynamics of photoexcitations in polydiacetylenes and polythiophene are thus related to the ultrafast nonlinear response dynamics. Their formation and relaxation processes are, therefore, quite essential and one of the most fundamental subjects to be investigated. The change is induced not only by the localized electronic excitation but also by vibrational excitation coupled to the electronic excitation through vibronic coupling start to modulate the molecular structure [12–15]. The structural modulation changes the energy-level scheme and the transition probability. The former changes the electronic spectrum and hence the intensity at some specific probe wavelength. The latter modulates the intensity in the way in the relevant homogeneous spectral range.

In the present Letter, the delay time dependence of difference absorbance and time-resolved spectrum is shown in Section 3.1, and the effect of the electronic transition spectrum by molecular vibration is discussed in Section 3.2. Initial phases of the

* Corresponding authors at: Advanced Ultrafast Laser Research Center, University of Electro-Communications, 1-5-1, Chofugaoka, Chofu, Tokyo 182-8585, Japan. Fax: +81 42 443 5825.
E-mail addresses: kobayashi@ils.uec.ac.jp (T. Kobayashi), dujuan@mail.siom.ac.cn (J. Du).

0009-2614/$ - see front matter © 2013 Elsevier B.V. All rights reserved.
http://dx.doi.org/10.1016/j.cplett.2013.02.068

vibrational modes coupled to the electronic transition via impulsive excitation are used to identify the mode observed either to the ground state or to the excited state in Section 3.3. From the analysis of dynamics of the mean distribution energy of the vibration energy, the rate of the descending process of the vibrational ladder is calculated for several modes. Vibrational phase relaxation rate is also calculated form the FWHM of the Fourier spectrum in Section 3.4. Section 3.5 discusses the electronic phase relaxation is obtained from the data in the negative time range when the probe pulse proceeds the pump pulse.

2. Experimental

2.1. Sample

The sample polymer studied is poly[*o*-TFMPA([*o*-(trifluoromethyl)phenyl]acetylene)] (hereafter abbreviated as PTTPA), whose molecular structure is shown in the inset of Figure 1. It was synthesized in the following way: The monomer, *o*-TFMPA ([*o*-(trifluoromethyl)phenyl]acetylene) was prepared according to the procedure by Okuhura [16]. Polymerization of the monomer was carried out under dry nitrogen. It was initiated by 1:l mixtures of WCl, or MoCIS with various organometallic cocatalyst (mixture of WCl, with Ph4Sn) and achieved molecular weights as high as 160 kDa (this is unit for molecular weight). Metal carbonyl based catalysts were prepared by irradiation of carbon tetrachloride solution of a metal carbonyl with UV light (200-W high-pressure Hg lamp, distance 5 cm) at 30 °C for 1 h. A mechanically strong film could be obtained by solution casting. The polymer was thermally fairly stable in air. The high molecular weight, film formation, and fair thermal stability of the present polymer are notable characteristics, which are not seen in poly(phenylacety1ene).

The polymerization using a WCl_6 or $MoCl_5$ catalyst was made to achieve a high (80–100%) yield. The polymers have molecular weights significantly larger than 10^6, and therefore, contain 10^4 repeat units in a chain. The synthesis and various chemical properties of the conjugated polymers are described and discussed in detail elsewhere [16,17].

2.2. Ultrafast spectroscopy

Using the 6.8 fs pulse, the pump induced absorbance change (ΔA) in PTTPA file sample was measured at 128 different wavelengths from 529 to 726 nm (2.34–1.71 eV) [18,19]. The pump and probe beams were both from the non-collinear parametric amplifier (NOPA), which is reported in detail in Refs. [18,19]. In brief description, the pump source of the NOPA system is a commercially supplied regenerative amplifier (Spectra Physics, Spitfire). The central wavelength, pulse duration, power of the output, and repetition rate of this amplifier were 800 nm, 50 fs, 740 mW, and 5 kHz, respectively. The output pulse from the NOPA was compressed with a compressor composed of a pair of prisms and a set of two chirp mirrors. The polarizations of the pump and probe beams were parallel to each other.

The pump–probe experiment setup was described in detail in our Refs. [20–23]. The pump–probe signal was spectrally dispersed with a polychromator (JASCO, M25-TP) over 128 photon energies (wavelengths) from 1.65 to 2.23 eV (753–555 nm). It was detected by 128 sets of avalanche photodiodes and lock-in amplifiers with a reference from an optical chopper intersecting the pump pulse at the repetition rate of 2.5 kHz.

3. Results and discussion

3.1. Delay time dependence of difference absorbance and time-resolved spectrum

Figure 1 shows the absorption, spontaneous fluorescence, and stimulated emission spectra. The last one is calculated from the spontaneous emission spectrum of the polymer sample. The laser spectrum also shown in the figure is overlapping with the tail of the absorption. Figure 2a shows the traces of difference absorbance $\Delta A(t)$ at 10 different probe photon energies. In the absorbance traces shown on the left hand side of Figure 2a, the electronic and vibrational effects are both apparent. The former appears as slow changes, which decay slowly due to the electronic relaxation. The latter effect appears as rapid modulation of the transition due to molecular vibration.

The time trace signals depicted in red color lines in Figure 2a are the multiplied traces by appropriate factors to show the modulation due to molecular vibration in the traces more clearly. Figure 2b shows the Fourier power spectra of $\Delta A(t)$ traces at the 10 different probe photon energies corresponding to the real-time traces in Figure 2a.

To investigate the mechanism of electronic relaxation, we first analyze the change of spectral shape during relaxation and then decay dynamics using analytic functions. Figure 3a shows the time-resolved spectrum integrated for 100 fs delay time duration with the center delay times between 100 and 1700 fs with a 100-fs step. For example, the spectrum at the center delay time of 400 fs is the time-resolved spectrum integrated over the 351–450 fs range. To see the change in the spectrum better, the time-resolved spectra normalized to the peak intensity are shown in Figure 3b. The spectral shit is to be discussed later in this Letter

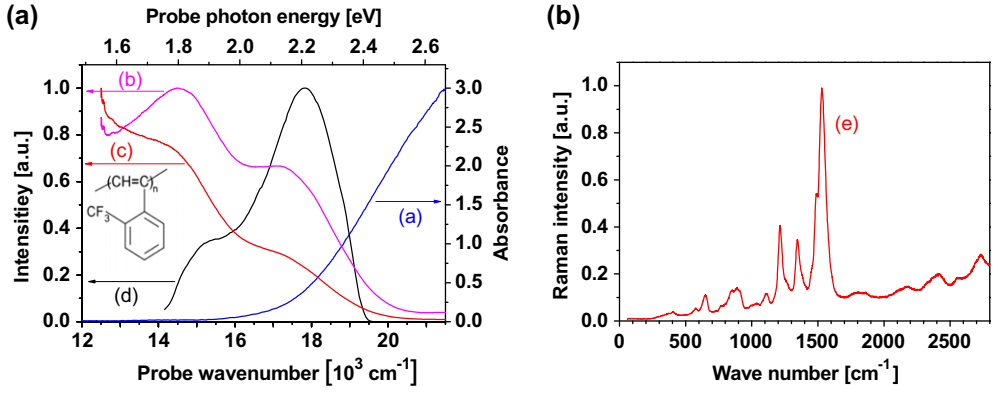

Figure 1. (a) Absorption, (b) spontaneous fluorescence, and (c) stimulated emission spectra of the PTTPA film sample and (d) the 6.8-fs laser spectrum. Inset is the molecular structure of PTTPA. Raman spectrum of PTTPA excited at 442 nm is depicted in (e).

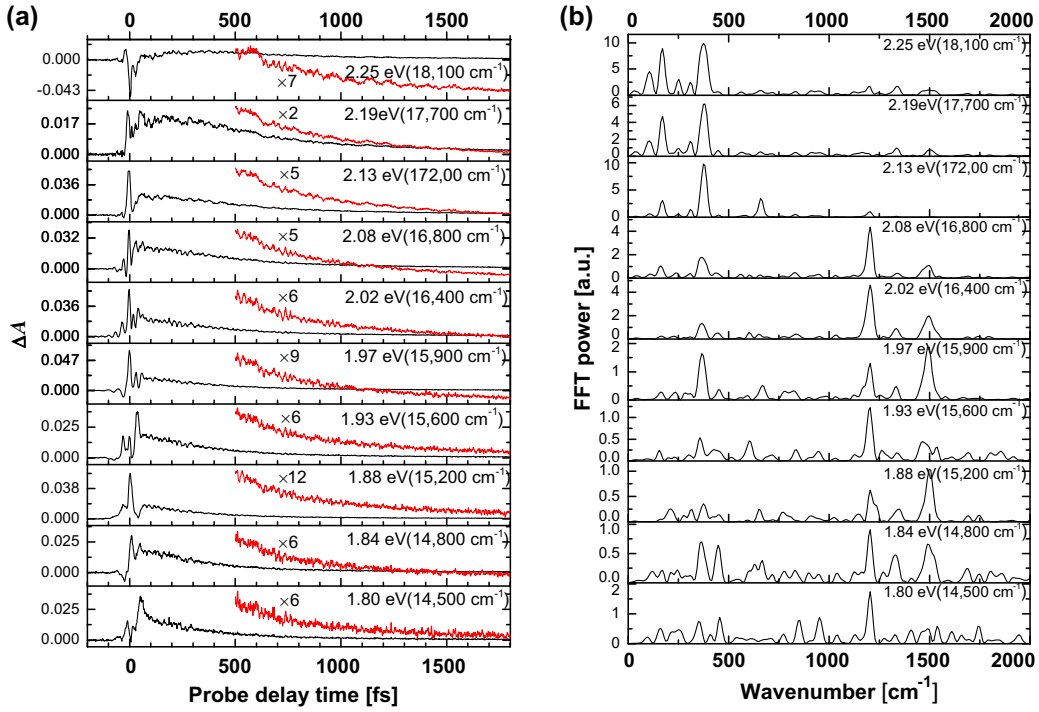

Figure 2. (a) Pump–probe delay time dependence of absorbance changes at 10 typical probe photon energies from −200 to 1800 fs. Magnified curves from 500 fs with appropriate magnification factors are also shown to clarify the molecular vibrations. (b) FFT amplitude spectra made by subtracting an exponential function from each real-time trace and taking FFT from 200 to 1800 fs.

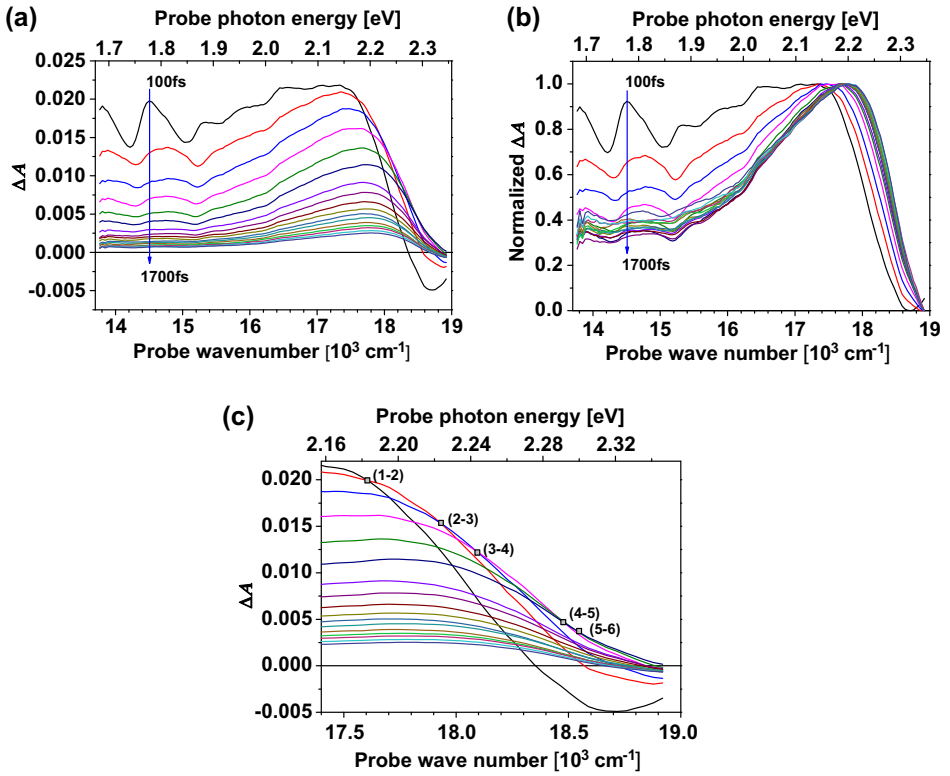

Figure 3. (a) Time-resolved spectrum integrated for 100 fs delay time duration with the center delay times between 100 and 1700 fs with a 100-fs step from the highest peak to the lowest peak. (b) Normalized spectra of (a). (c) Enlarged spectra from (a) to show the crossing points between the two neighboring delay times.

in terms of vibrational relaxation. Compared the time-resolved spectra with previous studies [24,25] of conjugated polymers, it can be concluded that dominant positive $\Delta A(t)$ in the whole spectral range of measurement is attributable to induced absorption

from free excitons at short delay time and then to the self-trapped excitons at longer delay time except in the probe frequency range higher than ~2.33 eV (18 800 cm^{-1}).

The two-dimensional difference absorption spectrum in the pump–probe delay time range from −200 fs to 1800 fs is shown in Figure 4a. Figure 4b shows the two-dimensional Fourier power spectrum of $\Delta A(t)$, which is calculated for the time range of 50–1800 fs. The time range shorter than 50 fs is not included in the calculation to avoid the effect of coherent effect between the scattered light of pump pulse and the probe pulse. Since the spectra in Figure 3a and b are all integrated for 100-fs span, the effect of the spectral shift and the intensity due to molecular vibration is substantially reduced because the integration smears out the spectral shifting associated with the molecular vibration. The crossing points between the neighboring delay-time steps of 100 fs are shown Figure 3c with the numbers of the participating delay times. The energies of the crossing points in 100–200, 200–300, 300–400, 400–500, and 500–600 fs descend rapidly from 2.18 to 2.31 eV (corresponding to 17 600–18 600 cm^{-1}). After 600 fs, the crossing points are heavily congested around 2.33 eV (18 800 cm^{-1}), indicating that the spectral shift becomes much slower than the preceding delay time. The normalized spectrum in Figure 3b shows a rapid blue shift of the whole spectrum from the delay time just after excitation until the central delay time of ~400 fs. The spectral shape is also changed rapidly in the same time range.

By the global fitting in the spectral range of 2.10–2.25 eV, two time constants were determined to be $\tau_1 = 20 \pm 2$ fs and $\tau_2 = 320 \pm 50$ fs. The former corresponds to the ultrafast geometrical relaxation from free excitons to self-trapped excitons in PTTPA in the absence of a barrier between them. The latter one, which is too short to be assigned to the population decay of STEs, namely the electronic population decay [24,25], is ascribed to the vibrational relaxation. Therefore, this blue-shift can be explained in terms of the intra-chain thermalization process in which the vibrational quanta of modes with high vibrational frequencies are scattered, being converted to low-frequency modes via vibrational mode coupling. It results in the reduction of the mean vibrational energy of the population distributed over vibrational levels with many modes and with different quantum numbers in the electronic excited state, which is the initial state of the transition with positive ΔA. The dynamics of the process can be studied by using the average transition energy in the positive ΔA regions calculated by the first moment of the transition energy; this is discussed later in Section 3.4. The blue shift can be ascribed to the change in the induced absorption caused by that of the population distribution in the lowest excited state (i.e., the initial state of the observed transition in the induced absorption) without change in the energy position of the vacant higher excited state (the final state of the transition). See the discussion in later sections on the relaxation process from the viewpoint of the vibronic coupled signals.

3.2. The effect of the electronic transition spectrum by molecular vibration

As described in Section 3.1, Figure 2a shows the traces of difference absorbance $\Delta A(t)$ as a function of the probe delay time at 10 different probe photon energies. The traces show a highly modulating signal on top of the slowly varying absorbance change, $\Delta A(t)$, due to electronic dynamics. The former rapid modulation in $\Delta A(t)$, represented by $\delta\Delta A(t)$, is due to a change in the transition spectra and/or those in the ground-state bleaching, stimulated emission, and excited-state absorption. This can be explained in terms of the stimulated Raman interaction described as Λ-type in the ground state or the Raman-like interaction described as V-type in the excited state of the spectral components corresponding to the pump and Stokes component [22]. The Fourier power spectra of the time-resolved modulation $\delta\Delta A(t)$ at the corresponding photon energies to the real-time traces in Figure 2a are shown in Figure 2b.

The signals of real-time vibration can be contributed from various mechanisms, as described below.

The first one arises from spectral changes including both intensity and shape due to the wavepacket motions in the ground and excited states. The intensity change at a specific probe wavelength can be due to the oscillation of the coefficients of the wavefunction of the wavepacket, which is a linear combination of vibrational eigenfunctions. Non-condon effect can also be the origin of the intensity change. These correspond to the imaginary part of the nonlinear susceptibility of the pump–probe process.

Another contribution is induced by the molecular phase modulation, MPM, caused by a kind of third-order nonlinear effect described by the molecular vibration-induced Kerr effect [26]. This may be interpreted as a kind of cross-phase modulation (sometimes called XPM), where the refractive index is modulated in proportion to the vibrational amplitude, which in turn is proportional to the pump laser intensity. This effect corresponds to the real part of the nonlinear susceptibility. The observed spectral change due to this mechanism is simply described by

$$d\Delta A = (d\Delta A(\omega)/d\omega)d\omega. \quad (1)$$

The effects of Raman and Raman-like contributions with high frequencies are not included in this equation, since they are out of the probe-frequency range of the moment calculation in the case of high-frequency mode. As for the modes of lower frequencies, they are included because of the above type of contributions.

From Eq. (1), the dependence of the Fourier amplitude on the probe photon energy is expected to be given by the first derivative

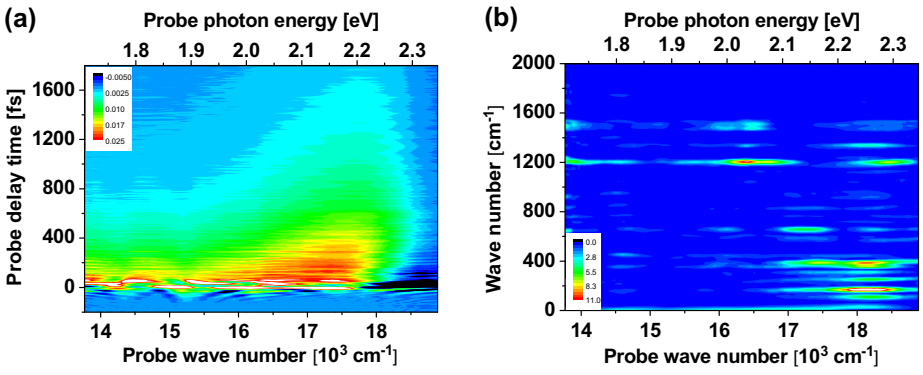

Figure 4. (a) Two-dimensional difference absorption spectrum. (b) Two-dimensional spectrum of FFT power of the difference absorption spectrum.

of the $\Delta A(\omega)$ spectrum if the wavepacket moves on the ground state potential modifying the stationary absorption spectrum of the ground state.

3.3. Initial phases of the vibrational modes coupled to the electronic transition via impulsive excitation

The initial phase of the molecular vibration is important for the assignment of the wavepacket responsible for the coherent modulation of the electronic transition intensity to either the excited state or the ground state. Figure 5a–h depict the dependence of the initial phase and the Fourier power of molecular vibration on the probe photon energy obtained by the FT of the time-dependent difference absorbance from 50 to 1800 fs.

As for the 106 cm^{-1} data shown in Figure 5a, the phases are $(-1/2)\pi$ in the full range of observation except in the probe-photon energy range between ~2.02 and ~2.05 eV (~16300 and ~16500 cm^{-1}), where the Fourier power is relatively small. It can be safely concluded from this phase dependence that the mode with 106 cm^{-1} is mainly attributed to the ground-state wavepacket. The frequency of this mode is too low for easy detection by conventional Raman spectroscopy, but this mode can be observed very clearly. This is the advantage of real-time vibrational spectroscopy, which is not suffered from intense Rayleigh scattering. In the same way, the mode with 114 cm^{-1} shown in Figure 5b is well attributed to the excited state except in the spectral range around 2.00 and 2.35 eV (16100 and 18950 cm^{-1}). Figure 5c shows the third lowest frequency of 171 cm^{-1}. In this case, all the initial phases calculated are close to π ranging between 1.97 and 2.35 eV (15900 and 18950 cm^{-1}) except in the range of 1.75 and 1.85 eV. From these phases the wavepacket generating modulation with 171 cm^{-1} can be assigned to the excited state. The modulation in the range of 1.75 and 1.85 eV is considered to be mixed with the signal induced by the excited wavepacket. In the same way, the mode with 244 cm^{-1} shown in Figure 5d is also due to the mixed contribution of the ground and excited states. The mode with 651 cm^{-1} depicted in Figure 5g has a peculiar feature of oscillating spectral Fourier power in the full probe range. The phases are all close to 0 π around 1.77 eV, 1.85, 2.05, and 2.26 eV (14300, 14900, 16500, and 18200 cm^{-1}), which are close to the peak positions of the FT power spectrum of this mode. Therefore, the signals corresponding to the peaks are dominantly due to the wavepacket in the excited state. The phase shown in Figure 5h is close to $-\pi/2$ near their FT power peaks around 2.0 and 2.3 eV. Therefore, the mode having large amplitude is concluded to be mainly due to the ground state. In the other probe range, the contribution from the excited state also has some sizable amount.

For discussion on the vibrational assignment of the peaks observed in the Fourier amplitude spectra, the frequencies of the Raman spectrum and those obtained by the FT of the real-time traces are listed together in Table 1. The Raman spectral pattern using the Ar laser, shown in Figure 1b, is quite different from that by the FT of real-time vibrational spectroscopy. This difference can be attributed to that of the resonance conditions in the excitation processes and the effect of the contribution of the wavepacket in the excited state. There are two more reasons for the difference: For low-frequency modes, it is due to the difficulty in observation of Raman signals, while for high-frequency modes the FT amplitudes obtained from real-time traces are reduced by a factor of $\left[(2\pi/t_p)^2/\left((\omega_m)^2+(2\pi/t_p)^2\right)\right]$ [23], where ω_m is the vibrational angular frequency of mode m and t_p is the pulse duration.

3.4. Vibrational-energy ladder descending process and vibrational-phase relaxation

For a detailed study of the vibrational-energy relaxation process associated with the thermalization discussed in Section 3.1, the first moment of the induced absorption was calculated in the integration range of 529–726 nm (2.34–1.71 eV). As shown in Figure 6, the decay of the moment corresponding to the average transition energy reduces gradually with the delay time t_D. This trend can be reproduced by the following fit to the calculated first moment:

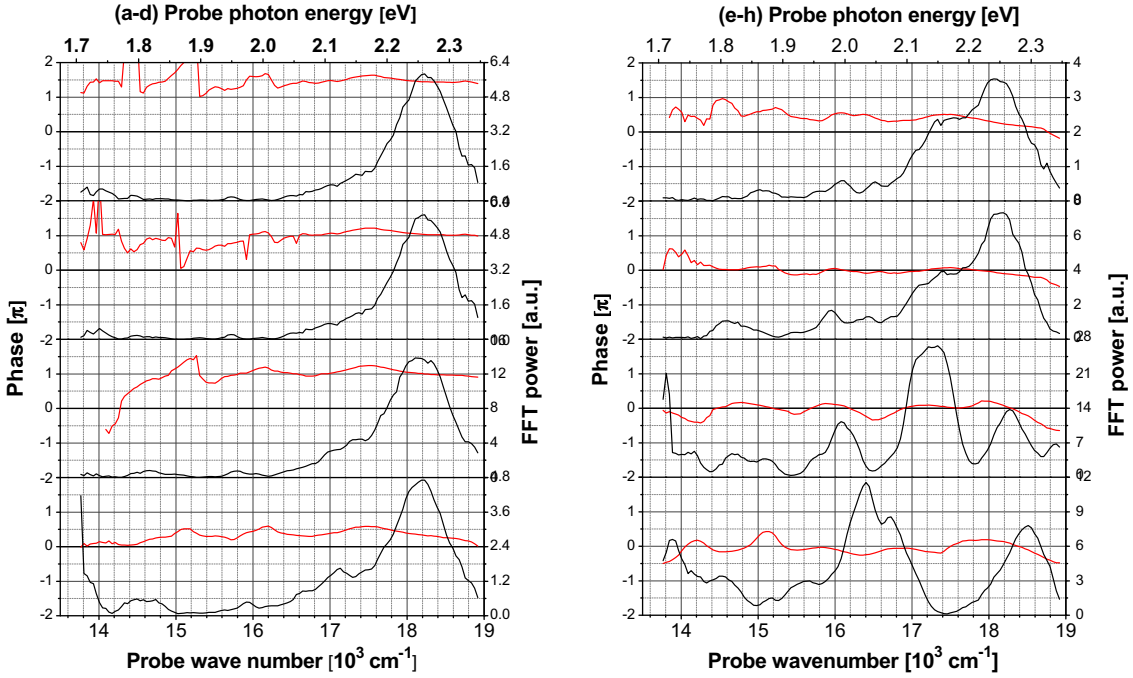

Figure 5. Probe photon energy dependencies of the initial phase (red) and FFT power (black) of molecular vibration for (a) 106, (b) 114, (c) 171, (d) 244, (e) 309, (f) 366, (g) 651, and (h) 1205 cm^{-1} obtained by the FFT of the time-dependent difference absorbance from 50 to 1800 fs. (For interpretation of the references to color in this figure legend, the reader is referred to the web version of this article.)

Table 1
Peaks in the Fourier amplitude spectra of vibrational modes obtained in the negative and positive ranges of ΔA compared with those observed in the Raman scattering spectrum using the excitation wavelength of 441.92 nm. (w: weak, m: middle, s: strong)

DA > 0		DA < 0		Raman (cm^{-1}) excited at 442 nm
Wavenumber (cm^{-1})	Normalized FFT power	Wavenumber (cm^{-1})	Normalized FFT power	
106	0.34	114	0.38	
171	0.66	171	0.69	
244	0.23			
		260	0.50	
309	0.27			
366	1			
		399	1	404.64(w)
448	0.34			
		578	0.37	576.0(w)
651	0.20	659	0.35	648.0(w)
		757	0.18	768.8(w)
				850.0(w)
				878.9(w)
				1108.4(w)
1201	0.85	1203	0.67	1211.5(m)
1335	0.20			1345.1(m)
1465	0.24			
		1497	0.30	1489.5(m)
		1530	0.25	1529.1(s)

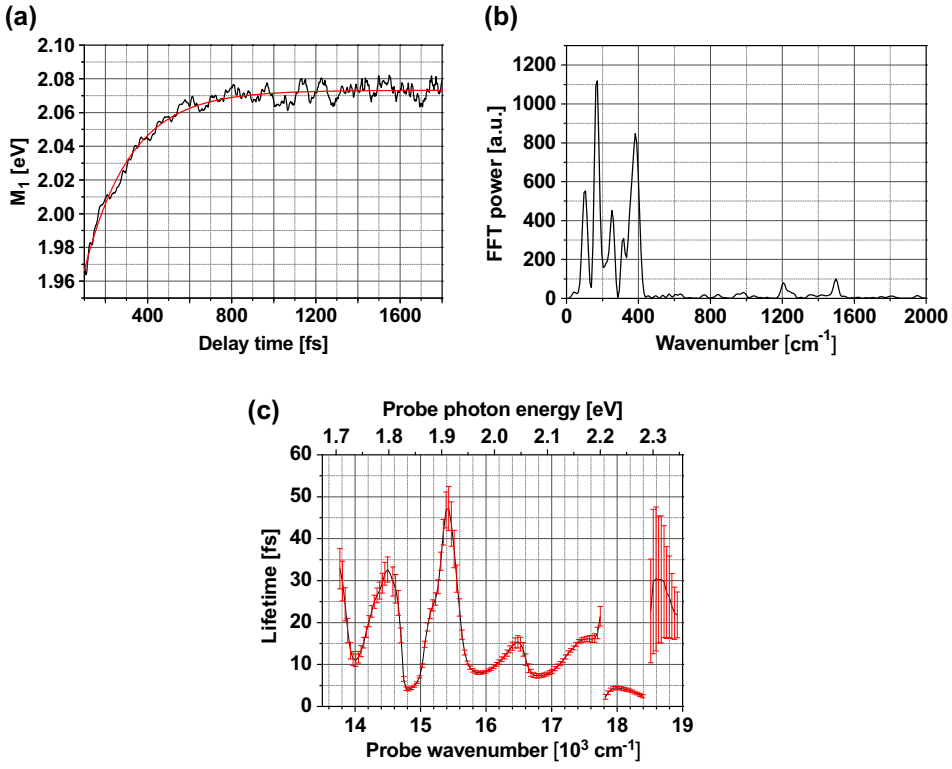

Figure 6. (a) Delay time dependence of the first moment (M_1) of the induced absorption spectra calculated by integrating in the range of 529–726 nm (2.34–1.71 eV). Curve M_1 is smoothed over the probe delay range of 10 fs. Fitting to an exponential curve is also displayed. (b) FFT of the (a) curve after the fitting curve is subtracted from the experimental curve. (c) Decay times of the signal in the negative time range as a function of the probe photon energy.

$$\Delta E(t_D) = (\Delta E - \Delta E_0)\exp(-t_D/\tau_e) + \Delta E_0 \quad (2)$$

where the relaxation time, τ_e, the initial extra energy, ΔE, and the final energy after thermalization, ΔE_0, were taken as variable parameters. From the best fit to the observed curve, the parameters were found to be $\tau_e = 217 \pm 2$ fs, $\Delta E = 1.91 \pm 0.01$ eV, and $\Delta E_0 = 2.08 \pm 0.01$ eV.

The fitted curve was then subtracted from the observed curve of the first moment to calculate the FT after normalization of all the peak intensities in the FFT spectra by the maximum peak at 171 cm^{-1}. The corresponding vibrational dephasing time was calculated from the bandwidth of each mode shown in Figure 6b. Six most intense vibrational modes with wavenumbers of 103, 171, 258, 383, 1201, and 1499 cm^{-1} can be observed in the normalized FFT spectrum in Figure 6b. The Fourier power associated with the mean energy (first moment) reducing with time provides the strength of the vibronic coupling which induces (mean) energy reduction. The modulations shown in the (mean) energy relaxation

obtained by the first moment is the total effect contributed from each vibrational mode. Therefore, the first moment can be expressed by the individual contribution from each mode (ΔE_{vi}) as

$$M_1(t_D) = \Delta E(t_D) + \sum_i \Delta E_{vi} \exp(-t_D/T_{2i}^{vib}) \cos(\omega_{vi} t_D + \varphi_i), \quad (i = 1,\ 2, \ldots,\ 6) \tag{3}$$

where ω_{vi} is the vibrational frequency of each mode, T_{2i}^{vib} is the vibrational dephasing time, and φ_i is the initial phase. The individual contribution to the energy relaxation can be obtained from each of the six modes, out of all the modes including those not well observed under the noise level using their relative peak values in the FT power spectrum in Figure 6b, in combination with the total amount of the energy relaxation in the excited state, obtained from the first moment of induced absorption. Using the individual contribution divided by the vibrational frequency of itself, the Huang–Rhys factors corresponding to the transition from the lowest to the higher excited states for these six modes can be determined as listed in Table 2. This is the first determination of multi-dimensional Huang–Rhys factors; the data of these multi-dimensional values provide the structure of the multi-dimensional potential hypersurface of complex molecular and polymer systems.

3.5. Electronic phase relaxation obtained from the data in the negative time range

In pump–probe spectroscopy, the pump pulse perturbs the absorption spectrum of the medium, which is subsequently probed after a set time delay. This method implicitly assumes that the weak probe pulse does not induce any substantial excitation of the sample [27]. In the femtosecond regime, however, the difference absorption spectra cannot be directly interpreted as a change in the absorption spectrum because of coherence effects. These effects fall into two categories: One is 'coherent coupling' due to the induced grating formed by the temporally coincident pump and the probe in the sample [27–30], and the other is the 'perturbed free polarization decay' generated by the probe and perturbed by the pump. In previous reports [27–34], the experimental results observed in the negative delay-time region were discussed in terms of perturbed free induction decay and coherent coupling. The difference absorption spectrum was calculated for a two-level system and applied to molecular systems [35,36]. We have here modified their treatment for the vibronic system in the following way: under the assumption that only one mode is coupled to the excitation to the exciton state but that it can readily be extended to a multi-mode system.The apparent absorbance difference, $\Delta A(\omega)$, observed in the negative time range in the rotating reference frame using the pump, $E_{pu}(t)$, and probe, $E_{pr}(t)$, fields is given by [37]:

$$\Delta A(\omega) \sim \mathrm{Im}\{[f_2(\omega)/e_{pr}(\omega)]\mathcal{F}[\boldsymbol{E}_{pu}(t)[F_1(t) \otimes (\boldsymbol{E}_{pu}^{*}(t)\boldsymbol{P}_{pr}(t))]]\} \tag{4}$$

Here $\boldsymbol{P}_{pr}(t)$ is the macroscopic polarization in a molecular vibronic system propagating in the probe direction, $f_2(\omega) = \mathcal{F}[F_2(t)]$ is the FT of:

$$F_2(t) = (i\mu/\hbar)\exp(-t/T_2^{el})\exp(-i\Omega t)\exp(-t/T_2^{vib})\exp(-i(\omega t + \phi)) \tag{5}$$

$$\boldsymbol{F}_1(t) = (2i\mu/\hbar)\exp(-t/T_1)\exp(-i(\omega t + \phi)) \tag{6}$$

$$\phi = \arctan[(\omega - \omega_{ba} + \omega_v)T_2^{vib}] \tag{7}$$

Here, T_2^{el} and T_2^{vib} are the electronic and vibrational dephasing times, respectively, and ω is the optical angular frequency corresponding to the 0–0 transition energy from the ground state to the electronic excited state. The symbol $\otimes$ denotes convolution; μ is the transition dipole moment; T_1 is the longitudinal electronic relaxation time; $\Omega = \omega_{ba} - \omega_1$ is the detuning between the pump field frequency ω_1 and the transition frequency ω_{ba}; ω_v is the vibrational angular frequency.

This perturbed free polarization decay term represents the case when the probe pulse arrives earlier than the pump pulse and there is no temporal overlapping between them. The probe pulse generates electronic coherence in the sample with the duration of the electronic dephasing time. Then the intense pump field forms a grating, i.e., $\boldsymbol{E}_{pu}^{*}(t)\boldsymbol{P}_{pr}(t)$ term in Eq. (4), which interacts with another pump field to be diffracted into the probe direction, satisfying the causality. In the present case, the vibronic coupling expected to be strong in the conjugated electron system is the origin of the electronic spectrum of the ground state. Therefore, the polarization generated by the probe pulse that precedes the pump pulse is a vibronic transition, instead of pure electronic transition, which is associated with the transition between the ground vibrational level in the ground electronic state and the vibronically excited state. The wave-packet formation in the ground state requires two fields of the pump pulse. Therefore, this signal increases with the delay time and the time constant T_2 and disappears quickly at $t = 0$ [30].

The decay times of the signal in the negative time range are functions of the probe photon energy, as shown in Figure 6c. The apparent lifetimes depend on the contribution of the coherent spike, which reduces the real dephasing time. The longest among the observed values is estimated to be the closest to the true value 47 ± 5 fs around 1.91 eV in the figure. This is a reasonable duration of dephasing in condensed phase materials [37].

Table 2
Lifetimes and Huang–Rhys factors of the vibrational modes determined from the first moment of ΔA.

Peak wavenumber (cm^{-1})	Normalized FFT power	Lifetime τ_{M1vib} (ps)	Huang–Rhys factor
M1			
49	0.026	1.67	
103	0.492	1.69	0.25
171	1	1.96	0.15
219	0.17	1.42	
258	0.415	1.78	0.10
313	0.273	2.21	
383	0.765	1.15	0.11
1201	0.071	1.80	0.01
1252	0.028	1.63	
1355	0.016	1.75	
1424	0.013	1.21	
1499	0.089	1.26	0.01
1550	0.011	2.01	

4. Conclusions

By utilizing the pump–probe data in the negative time range with sub-7 fs pulses, we have obtained the electronic phase relaxation time and the frequencies of the vibrational modes due to the wavepacket motion in the electronic excited sate. The absorbance change observed in the 'negative' time range has been used for estimation of the electronic dephasing time to be 47 ± 5 fs. Coherent molecular vibration of a polymer in the excited state has been observed in the real-time trace without the effect of wave packet motion in the ground state, which usually hinders assignment of the signal to either the ground state or the excited state.

Acknowledgments

This work was supported by the National Science Council of the Republic of China, Taiwan (NSC 98-2112-M-009-001-MY3), and a Grant from the Ministry of Education, Aiming for Top University (MOE ATU) Program at National Chiao-Tung University (NCTU). A part of this work was performed under the joint research project of the Institute of Laser Engineering, Osaka University under Contract No. A3-01.

References

[1] T. Kobayashi (Ed.), Nonlinear Optics of Organics and Semiconductors, Springer Proceeding Physics, vol. 36, Springer, Berlin, 1989.
[2] A.J. Heeger, S. Kivelson, J.R. Schrieffer, W.-P. Su, Rev. Mod. Phys. 60 (1988) 781.
[3] S. Etemad, Z.G. Soos, in: R.J.H. Clark, R.E. Hester (Eds.), Spectroscopy of Advanced Materials, Wiley, New York, 1991, p. 87.
[4] R.H. Friend, R.W. Gymer, A.B. Holmes, J.H. Burroughes, R.N. Marks, C. Taliani, D.D.C. Bradley, D.A. Dos Santos, J.L. Brédas, M. Lögdlund, W.R. Salaneck, Nature 397 (1999) 121.
[5] F. Hide, M.A. Díaz-García, B.J. Schwartz, A.J. Heeger, J. Acc. Chem. Res. 30 (1997) 4301.
[6] T. Kobayashi, IEICE Trans. Fundam. E75 (1992) 38.
[7] E.I. Rashiba, Excitons, Selected Chapters, in: E.I. Rashiba, M.D. Sturge (Eds.), Elsevier Science, Amsterdam, 1987, p. 273.
[8] T. Kobayashi (Ed.), Relaxation in Polymers, World Scientific, Singapore, 1993.
[9] A.J. Heeger, S. Kivelson, J.R. Schrieffer, W.P. Su, Rev. Mod. Phys. 60 (1988) 781.
[10] T. Kobayashi, M. Yoshizawa, U. Stamm, M. Taiji, M. Hasegawa, J. Opt. Soc. Am. B 7 (1990) 1558.
[11] T. Kobayashi, M. Yoshizawa, T. Masuda, T. Higashimura, T. Kobayashi, IEEE J. Quantum Electron. 28 (1992) 2508.
[12] H. Kano, T. Saito, A. Ueki, T. Kobayashi, Int. J. Mod. Phys. B 15 (2001) 3817.
[13] H. Kano, T. Saito, T. Kobayashi, J. Phys. Chem. A 106 (2002) 3445.
[14] T. Kobayashi, T. Teramoto, V.M. Kobryanskii, T. Taneichi, Synth. Met. 159 (2009) 1751.
[15] J. Du, T. Kobayashi, Chem. Phys. Lett. 481 (2009) 204.
[16] K. Okuhara, J. Org. Chem. 41 (1976) 1487.
[17] T. Masuda, T. Hamano, K. Tsuchihara, T. Higashimura, Macromolecules 23 (1990) 1374.
[18] A. Shirakawa, I. Sakane, T. Kobayashi, Opt. Lett. 23 (1998) 1292.
[19] A. Baltuska, T. Fuji, T. Kobayashi, Opt. Lett. 27 (2002) 306.
[20] T. Kobayashi, J. Zhang, Z. Wang, New J. Phys. 11 (2009) 013048.
[21] T. Kobayashi, A. Yabushita, Chem. Rec. 11 (2011) 99.
[22] J. Du, T. Teramoto, K. Nakata, E. Tokunaga, T. Kobayashi, Biophys. J. 101 (2011) 995.
[23] Y. Wang, T. Kobayashi, ChemPhysChem 11 (2011) 889.
[24] T. Kobayashi, A. Shirakawa, H. Matsuzawa, H. Nakanishi, Chem. Phys. Lett. 321 (2000) 385.
[25] T. Kobayashi, M. Hirasawa, Y. Sakazaki, H. Hane, Chem. Phys. Lett. 400 (2004) 301.
[26] N. Zhavoronkov, G. Korn, Phys. Rev. Lett. 88 (2002) 203901.
[27] C.H. Brito Cruz, R.L. Fork, W.H. Knox, C.V. Shank, Chem. Phys. Lett. 132 (1986) 341.
[28] J.J. Baumberg, B. Huttner, R.A. Taylor, J.F. Ryan, Phys. Rev. B 48 (1993) 4695.
[29] C.V. Shank, R.L. Fork, C.H. Brito Cruz, W. Knox, in: G.R. Fleming, A.E. Siegman (Eds.), Ultrafast Phenomena V, Springer, Berlin, 1986.
[30] C.H. Brito Cruz, J.P. Gordon, P.C. Becker, R.L. Fork, C.V. Shank, IEEE J. Quantum Electron. 24 (1988) 261.
[31] B. Fluegel, N. Peyghambarian, G. Olbright, M. Lindberg, S.W. Koch, M. Joffre, D. Hulin, A. Migus, A. Antonetti, Phys. Rev. Lett. 59 (1987) 2588.
[32] F.W. Wise, M.J. Rosker, G.L. Millhauser, C.L. Tang, IEEE J. Quantum Electron. 23 (1987) 1116.
[33] M. Lindberg, S.W. Koch, Phys. Rev. B 38 (1988) 7607.
[34] J.P. Likforman, M. Joffre, G. Chériaux, D. Hulin, Opt. Lett. 20 (1995) 2006.
[35] C.J. Bardeen, C.V. Shank, Chem. Phys. Lett. 203 (1993) 535.
[36] J.Y. Bigot, M.T. Portella, R.W. Schoenlein, C.J. Bardeen, A. Migus, C.V. Shank, Phys. Rev. Lett. 66 (1991) 1138.
[37] T. Kobayashi, J. Du, W. Feng, K. Yoshino, Phys. Rev. Lett. 101 (2008) 037402.